The 19th International Symposium on Magnetic Bearings
ISMB19 Digest

Current reference computation for Bearingless Multi-Sector Permanent Magnet Machine: methods and issues

Hugo MILAN*, Meiqi WANG**, Lorenzo CARBONE**, Antoine CIZERON*** and Javier OJEDA*
* Université Paris-Saclay, ENS Paris-Saclay, CNRS, SATIE, 91190, Gif-sur-Yvette, France
** Electrical and Electronic Engineering, The University of Nottingham, United-Kingdom
*** Universite Claude Bernard Lyon 1, Ampère, UMR5005, INSA Lyon, Ecole Centrale de Lyon, CNRS, 69100 Villeurbanne, France

1. Introduction

Bearingless Machines (BMs) combine the functions of Active Magnetic Bearings (AMBs) with those of traditional rotating electric machines, allowing for the simultaneous suspension of the rotor and the generation of torque [1]. Since their inception in the early 1970s, these machines have gained significant interest due to their benefits in high-speed applications, including reduced mechanical losses and enhanced reliability [1]. These attributes make them especially suitable for use in compressors, flywheels, turbo-molecular pumps, and high-speed generators [2], where minimizing system weight and maximizing efficiency are paramount [3]. Furthermore, their contact-free operation eliminates mechanical wear, making them an optimal choice for challenging environments such as vacuums, extreme temperatures, and sterile conditions [4].

A significant challenge in bearingless drives is the concurrent control of torque and radial forces. Conventional bearingless motors utilize two separate winding sets—one for generating torque and another for active force control [5]. An innovative alternative is the Multi-Sector Permanent Magnet (MSPM) machine, which employs a spatially distributed winding arrangement to facilitate simultaneous torque and force control using a three-phase winding set for each pole pair, supplied in an interdependent manner [6]. The Fig.1 examines an MSPM machine, which is based on a standard 18-slot, 6-pole Permanent Magnet Synchronous Machine (PMSM), but features a modified winding configuration. The multi-three-phase topology allows for a spatial distribution of conductors, enabling independent control of both $x-y$ force components and torque across distinct sectors. The machine's three-phase winding sets are powered by conventional inverters, coordinated through a unified control platform. This configuration offers benefits such as simplified machine construction, enhanced fault tolerance, and greater control flexibility. However, the strong cross-coupling between force and torque generation in MSPM machines presents additional control challenges, necessitating advanced strategies to ensure precise force regulation [7]. Within the control system, there are two key leverage points for achieving an effective control strategy. The first approach involves enhancing the computation of force and torque references from position and velocity measurements, which corresponds to improving the mechanical control loop [7]. The second approach focuses on refining the method for computing current references based on force and torque references. This study specifically explores improvements in the computation of current references from given force and torque references.

This work reviews the derivation of current references from force and torque inputs to enhance force precision in MSPM machines, bridging the mechanical controller and current control, as shown in Fig. 1.

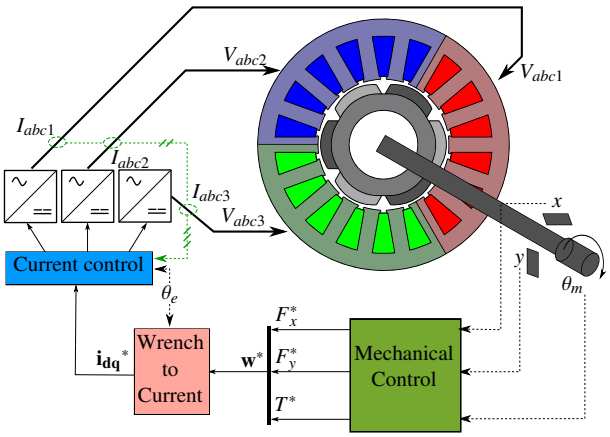

Fig. 1 Control diagram of MSPM

2. Resultant Force on the rotor

To understand how force is generated in a sectorized machine, it's essential to first examine why controlling the overall force on the rotor is not feasible in a conventional machine. The calculation of the force and the torque on the rotor is performed through the integration of the Maxwell stress tensor along the airgap circumference (cyan circle in Fig. 2). This method can be summarized in 3 steps :

(1) Calculation of the magnetic fields B and H along the airgap circumference.

(2) Calculation of surface force along the airgap circumference.

(3) Integration

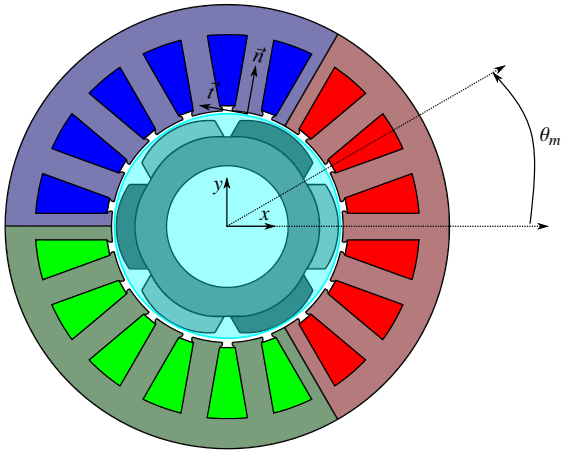

Fig. 2 Force on the rotor in MSPM

The normal and tangential components of the magnetic fields B and H relative to this circle are then calculated by the methods detailed in Section. 3.1. Using these fields, the surface force on the circle can be expressed using Equation 1:

$$\vec{f}(\theta_m) = \frac{1}{2}\left(\frac{\vec{B}(\theta_m)\cdot\vec{n}}{\mu_0}^2 + \left(\mu_0\vec{H}(\theta_m)\cdot\vec{t}\right)^2\right)\cdot\vec{n} + \frac{1}{2}\left(\vec{B}(\theta_m)\cdot\vec{n}\right)\left(\vec{H}(\theta_m)\cdot\vec{t}\right)\cdot\vec{t} = f_n(\theta_m)\cdot\vec{n}(\theta_m) + f_t(\theta_m)\cdot\vec{t}(\theta_m) \quad (1)$$

The resultant global force on the rotor is obtained by integrating the surface force over the entire surface of the circle. In a conventional machine, the magnetic field remains invariant under rotation by an angle corresponding to a pair of poles $\left(\frac{2\pi}{p}\right)$. Consequently, the surface force amplitude remains unchanged under such rotation:

$$\vec{f}\left(\theta_m + \frac{2\pi}{p}\right) = f_n(\theta_m)\cdot\vec{n}\left(\theta_m + \frac{2\pi}{p}\right) + f_t(\theta_m)\cdot\vec{t}\left(\theta_m + \frac{2\pi}{p}\right) = \mathbf{R}\left(\frac{2\pi}{p}\right)\vec{f}(\theta_m) \quad (2)$$

In Eq. 3 and 4, upon integrating the force over the surface of each pole pair, the same force amplitude is obtained but with a rotation of $\frac{2\pi}{p}$ for each pole pair.

$$\vec{F_i} = lr\int_{\frac{2\pi}{p}(i-1)}^{\frac{2\pi}{p}i}\vec{f}(\theta_m)d\theta_m \quad (3)$$

with i the sector index $i \in [1, p]$ and l the length of the rotor and r the radius

$$\vec{F_i} = \mathbf{R}\left(\frac{2\pi}{p}i\right)\vec{F_1} \quad (4)$$

Being $\Sigma_{i=1}^{p}\mathbf{R}\left(\frac{2\pi}{p}i\right) = \mathbf{0}$,

$$\sum_{i=1}^{p}\vec{F_i} = \vec{0} \quad (5)$$

As a result, the resultant force becomes zero in a conventional machine. In a sectorized machine, each pole pair can be powered differently, which breaks the rotational invariance and allows for the creation of a resultant force on the rotor. This leads to the question: What methods can be employed to determine the force induced by this unbalanced power supply for effective control ?

3. Current Reference Computation in Healthy Operation

In MSPM machines, the objective is to control the electromagnetic mechanical forces and torque exerted on the rotor. These quantities are collectively referred to as the wrench, denoted by **w**:

$$\mathbf{w} = \begin{bmatrix} F_x & F_y & T \end{bmatrix}' = \begin{bmatrix} \mathbf{F} & T \end{bmatrix}' \tag{6}$$

Here, the prime symbol $'$ represents the transpose operator. T signifies the torque acting on the rotor, while F_x and F_y are the components of the force decomposed in the x and y reference frame. Based on Fig. 2, these forces are determined using a plane that is perpendicular to the rotor, with its center aligned with the axial center of the rotor. To effectively control the MSPM machines, it is essential to establish a relationship between the wrench and the current. The most straightforward approach involves characterizing the torque and force for each possible sector excitation configuration.

3.1. Current to wrench model

To effectively control the MSPM machines, it is crucial to establish the relationships between the dq-axis currents of each sector, denoted as $({}^{i}i_d, {}^{i}i_q)$ where i identifies the sector, and their contributions to the overall wrench **w**. These contributions are dependent on both the sector currents and the rotor's electrical position, and can be expressed by the function:

$${}^{i}\mathbf{w} = \begin{bmatrix} {}^{i}F_x, {}^{i}F_y, {}^{i}T \end{bmatrix}' = {}^{i}f({}^{i}i_d, {}^{i}i_q, \theta_e) \tag{7}$$

Under linear operating conditions, the total wrench of the machine is the sum of the individual contributions from each of the N sectors:

$$\mathbf{w} = \sum_{i=1}^{N} {}^{i}\mathbf{w} = \sum_{i=1}^{N} {}^{i}f({}^{i}i_d, {}^{i}i_q, \theta_e) \tag{8}$$

To achieve precise control of the wrench, the initial step involves identifying the function ${}^{i}f$. There are two primary methods for this identification, as compared in [8], which are both based on the Maxwell tensor method:

(1) Finite Element Analysis (FEA)

(2) Analytical Model

For the FEA, the process begins with constructing a geometric model of the machine. Power supply scenarios are then defined, presenting two possible solutions. The first solution involves powering one sector with n types of power supplies while leaving all other sectors open-circuited. This approach assumes that each sector contributes equally, an assumption that holds true under the linear operating conditions of the machine. The second solution involves applying these power supply scenarios to all sectors, which results in n^N simulations. This method, however, becomes computationally intensive when dealing with three or more sectors. FE simulations are subsequently performed for these operating points, which correspond to the power supply scenarios. To obtain a function of currents and electrical angle, a model that fits these data is defined, with a linear model typically being chosen.

For the Analytical Model, detailed in [9], the process starts by establishing the relationship between phase power supplies and the magnetomotive force. Using the magnetomotive force in the air gap, the B and H fields in the air gap are calculated. Finally, the force applied to the rotor is determined.

Each method presents particular advantages and disadvantages, as summarized in Table 1. The Finite Element Analysis (FEA) offers high precision, capturing complex effects such as spatial harmonics due to its consideration of non-linearities and the non-infinite permeability of ferromagnetic materials. However, this accuracy comes with increased complexity and longer simulation times, making it less efficient in terms of computational demands and interpretability. The Analytical Model, while less precise due to its linear approach, is quicker to utilize once established. This makes it ideal for rapid calculations and for understanding the impact of various design parameters. Although it may overlook finer details like spatial harmonics, it provides better interpretability and faster computation times. But these two techniques will yield very similar results if the machine's behavior is within the linear range, as is the case in [8].

Both techniques provide a linear model that relates the current, expressed in the dq-axis, to the wrench, with a $3 \times 2N$ matrix:

$$\mathbf{w} = \mathbf{K_{dq}}(\theta_e)\mathbf{i_{dq}} \tag{9}$$

Given that $\mathbf{K_{dq}}(\theta_e)$ is not a square matrix, the next step involves finding an efficient method to invert or pseudo-invert this matrix to solve for the currents $\mathbf{i_{dq}}$. This is crucial for determining the appropriate current inputs needed to achieve the desired wrench outputs in the system.

	Acurracy	Model construction	Computation Time	Interpretability
Finite Element Analysis (FEA)	+	+	-	-
Analytical Model	-	-	+	+

Table 1 Strength and weakness of FEA et Analytical Model for force computation

3.2. Inversion technics

To address the inversion problem, two primary techniques have been considered:

(1) Decoupled torque and force control technique

(2) Pseudo-inverse Calculation

Decoupled torque and force control technique, proposed by Ooshima et al. in [10], takes advantage of the dq-axis modeling of PMSM machines. In this model, the torque demand and force vector are generated by controlling the N q-axis and d-axis components of the current in the synchronous reference frame, respectively. By leveraging the magnetically isotropic structure of the MSPM machine, torque control is achieved solely through the q-axis current components of each sector. The total q-axis current demand is derived from the torque expression given by equation 10:

$$T = \sum_{i=1}^{p} K_T {}^{i}i_q \Rightarrow {}^{i}i_q = \frac{T}{pK_T} \quad \text{with } K_T \text{ the torque coefficient.} \tag{10}$$

The transformation of the forces developed by each sector into rectangular force components on the overall rotor structure is introduced to reduce the complexity of the problem. Under the assumption that electromagnetic forces are related only to the d-axis current components, equations 10 and 11 define the complete model of the MSPM machine:

$$\begin{bmatrix} {}^{1}i_d \\ {}^{2}i_d \\ {}^{3}i_d \end{bmatrix} = \frac{2}{3K_F} \begin{bmatrix} 1 & 0 \\ -1/2 & \sqrt{3}/2 \\ -1/2 & -\sqrt{3}/2 \end{bmatrix} \begin{bmatrix} F_x \\ F_y \end{bmatrix} \quad \text{with } K_F \text{ the current-force coefficient.} \tag{11}$$

This technique relies on robust and reliable current control. The concepts of current loops and the decoupling of the d-axis and q-axis are well understood in both academic and industrial fields. Therefore, separating torque generation and force generation by decoupling the d-axis and q-axis prevents disturbances in one when the setpoint of the other is changed.

However, this technique suffers from a significant issue: the force generated by one sector changes as the electrical angle changes. This variation creates ripples in force generation, leading to ripples in position and causing disturbances in the mechanical loop. To address this issue, Ooshima et al. in [11] proposed adjusting the force reference according to the electrical angle. This correction assumes that the reference error, denoted as $\mathbf{F}^*$, is accurate for $\theta_e = 0$ and contains errors when $\theta_e \neq 0$. A complex coefficient $\underline{k_f}(\theta_e)$ is used to correct both the magnitude and the angle error. Thus, the reference force and the actual force are linked by the relation:

$$\mathbf{F} = \left|\underline{k_f}(\theta_e)\right| \mathbf{R}(\arg(\underline{k_f}(\theta_e)))\mathbf{F}^* \tag{12}$$

Since the relation is linear, the inverse linear relation in Eq. 13 is used to compute the corrected force $\mathbf{F}_\mathbf{c}^*$ for the current computation:

$$\mathbf{F}_\mathbf{c}^* = \frac{1}{\left|\underline{k_f}(\theta_e)\right|} \mathbf{R}(\arg(\underline{k_f}(\theta_e)))^{-1}\mathbf{F}^* \tag{13}$$

This technique, however, faces two significant issues. First, the correction data must be stored in a look-up table, which increases the memory requirements for a control system that previously required little memory space. Second, if $\underline{k_f}(\theta_e)$ is not well characterized, it can introduce additional ripples in the control loop.

The second technique, introduced by Giorgio et al. [8], is known as the Pseudo-inverse Calculation. This method utilizes the dq-axis framework to solve an optimization problem aimed at generating the desired force and torque. Since the matrix $\mathbf{K_{dq}}(\theta_e)$ is not square, there are infinitely many current references capable of producing the same wrench. The most widely adopted and elegant solution to this issue involves determining the current reference that minimizes Joule losses ($P_{J,tot}$):

$$\min P_{J,tot} = \mathbf{i}_\mathbf{dq}^{'} \mathcal{R}_s \mathbf{i}_\mathbf{dq} \text{ s.t. } \mathbf{w}^* = \mathbf{K_{dq}}(\theta_e)\mathbf{i_{dq}} \tag{14}$$

The solution to this optimization problem is given by:

$$\mathbf{i_{dq}} = \mathbf{K_{dq}}'(\theta_e)\left[\mathbf{K_{dq}}(\theta_e)\mathbf{K_{dq}}'(\theta_e)\right]^{-1}\mathbf{w}^* = \mathbf{K}^+_{\mathbf{dq}}(\theta_e)\mathbf{w}^* \tag{15}$$

In this context, $\mathbf{K}^+_{\mathbf{dq}}(\theta_e)$ denotes the pseudo-inverse matrix of $\mathbf{K_{dq}}$. A significant challenge with this technique lies in calculating $\mathbf{K}^+_{\mathbf{dq}}(\theta_e)$ due to the complexities involved in matrix inversion. Computing the pseudo-inverse matrix online is particularly demanding because of the extensive number of operations required, even when employing the Singular Value Decomposition (SVD) technique. To overcome this challenge, $\mathbf{K}^+_{\mathbf{dq}}(\theta_e)$ is precomputed offline and stored in the microcontroller using a lookup table. To minimize computational time associated with incremental memory access, the matrix can be stored by harmonics. Equation 16 illustrates the harmonic formulation for the pseudo-inverse, enabling selection of the matrix's harmonic richness. If the position ripple is excessively high, increasing the number of harmonics in the matrix can mitigate this issue. However, this adjustment also introduces additional harmonics into the current references, necessitating careful design of the current control system to accommodate this constraint.

$$\mathbf{K}^+_{\mathbf{dq}}(\theta_e) =^+ \mathbf{K^0_{dq}} + \sum_{n=1}^{+\infty} +\mathbf{K^{2na}_{dq}}\cos(2n\theta_e) + {}^+\mathbf{K^{2nb}_{dq}}\sin(2n\theta_e) \tag{16}$$

The two inversion techniques for MSPM machine control each have distinct benefits and challenges. The Decoupled Torque and Force Control Technique simplifies control by separating torque and force but introduces ripples and requires additional corrections. The Pseudo-inverse Calculation minimizes Joule losses and efficiently determines current references, but faces computational complexity. Choosing between them depends on specific application requirements, including computational resources and memory constraints.

3.3. Eccentricity Compensation

The main perturbation affecting force generation in these systems is the eccentricity of the rotor. According to [12], this perturbation can be expressed as :

$$\mathbf{w} = \mathbf{K_{dq}}(\theta_e)\mathbf{i_{dq}} + \mathbf{G}(\theta_\rho)\rho \tag{17}$$

where $\mathbf{G}(\theta_\rho)$ is a vector identified by either FE or analytical methods, depending on the angle of the eccentricity introduced in Fig. 3. The variable ρ represents the magnitude of the eccentricity.

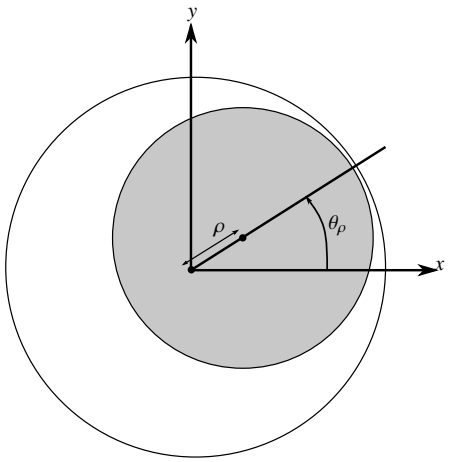

Fig. 3 eccentric rotor [9]

To counteract this perturbation, two solutions are employed:

- **Mechanical Loop Correction:** According to Eq. 17, the eccentricity acts as a perturbation on force generation. This perturbation is proportional to the error, so the controller must be designed based on the principles outlined in [13].
- **Explicit Correction in the Wrench Model:** By calculating the force-torque generated by the eccentricity using Eq. 17, it is possible to adjust the wrench reference. This method is detailed in [12].

Given that these systems are equipped with a safety bearing, the value of ρ is constrained to between 15% and 25% of the airgap length. This limitation caps the maximum force perturbation. Typically, the perturbation remains within the manageable range of the linear control system, making it controllable. However, to enhance system performance, it will be essential to compare the two methods and study their interactions.

4. Special Applications: Power-Sharing and Fault-Tolerant Control

Control systems for MSPM machines have significantly evolved, reaching a level of maturity that allows for the integration of advanced capabilities. This includes the implementation of power-sharing and fault-tolerant control.

4.1. Power-Sharing in Modular MSPM Machines

In power-sharing configurations, multiple inverter modules independently supply different winding sectors. Unlike traditional control schemes, which assume uniform power distribution, power-sharing strategies dynamically allocate current among sectors to balance loads and improve efficiency [14, 15]. This control strategy for the MSPM machine is based on the fact that force generation consumes a negligible amount of energy compared to torque generation. For example, the machine used in [15] has a nominal power of 5 kW for torque generation, but the rotor displacements are on the order of 100 micrometers, and the machine's weight is 20 N, resulting in a power magnitude on the order of 2 mW for force generation.

To implement this control, a modified force-to-current transformation matrix that accounts for non-uniform sector contributions is required. A new optimization problem must be solved:

$$\min P_{J,tot} = \mathbf{i}_{\mathbf{dq}}^{'}\mathcal{R}_s\mathbf{i}_{\mathbf{dq}} \text{ s.t. } \mathbf{w}^* = \mathbf{K}_{\mathbf{dq}}(\theta_e)\mathbf{i}_{\mathbf{dq}} \text{ s.t. } \mathbf{i}_{\mathbf{q}} = \mathbf{z}^* \frac{T}{K_T} \tag{18}$$

where $\mathbf{z} = \begin{bmatrix} z_1 & z_2 & z_3 \end{bmatrix}$ are the power-sharing parameters and $\mathbf{i}_{\mathbf{q}} = \begin{bmatrix} i_{q1} & i_{q2} & i_{q3} \end{bmatrix} = \begin{bmatrix} z_1 & z_2 & z_3 \end{bmatrix} \frac{T}{K_T}$, to reach the desired torque $z_1 + z_2 + z_3 = 1$. The solution to this problem is:

$$\mathbf{i_d} = \mathbf{K_d}'(\theta_e)\left[\mathbf{K_d}(\theta_e)\mathbf{K_d}'(\theta_e)\right]^{-1}\left(\mathbf{F} - \mathbf{K_q}(\theta_e)\mathbf{i_q}\right) \tag{19}$$

where $\mathbf{K_d}$ and $\mathbf{K_q}$ are analogous to $\mathbf{K_{dq}}$ for the d-axis and q-axis, respectively.

In power-sharing conditions, the choice of $\mathbf{z}^*$ allows for the selection of the q-axis current values. Since the power of the machine is primarily due to torque and rotational speed, the choice of q-axis current allows for the regulation of power flow in each sector. However, the imbalance of q-axis currents creates a force, so the force reference in Eq. 19 is corrected with the force created by the q-axis current. Thus, the pseudo-inverse is not the same as in the healthy scenario, but the issues associated with calculation and implementation remain unchanged.

4.2. Fault-Tolerant Control: Handling Open-Circuit Failures

The sectorization, independent power supply for each set of three-phase windings, and low coupling make the MSPM machine a strong candidate for fault-tolerant applications [16]. In these applications, while the bearingless feature is not implemented, the redundancy allows the system to handle various electrical faults such as open-circuit and short-circuit conditions. However, for bearingless applications, the most commonly addressed fault type in the literature is an open-phase condition, where one or more phases in a sector are open-circuited [15, 17]. To implement control under open-circuit conditions, a new optimization problem must be solved. However, since the machine is characterized in the dq-axis framework, handling a single-phase open-circuit is challenging. To circumvent this issue, when a single phase is open, all three phases of the sector are opened. In Equation 21, the new optimization problem is stated for the scenario where sector 1 is open-circuited:

$$\min P_{J,tot} = \mathbf{i}_{\mathbf{dq}}^{'}\mathcal{R}_s\mathbf{i}_{\mathbf{dq}} \text{ s.t. } \mathbf{w}^* = \mathbf{K}_{\mathbf{dq}}(\theta_e)\mathbf{i}_{\mathbf{dq}} \text{ s.t. } {}^1i_d, {}^1i_q = 0 \tag{20}$$

Since sector 1 cannot produce force, a new formulation can be stated as:

$$\min P_{J,tot} = \begin{bmatrix} {}^2i_d & {}^2i_q & {}^3i_d & {}^3i_q \end{bmatrix}\mathcal{R}_s \begin{bmatrix} {}^2i_d \\ {}^2i_q \\ {}^3i_d \\ {}^3i_q \end{bmatrix} \text{ s.t. } \mathbf{w}^* = \mathbf{K_{OC}}(\theta_e) \begin{bmatrix} {}^2i_d \\ {}^2i_q \\ {}^3i_d \\ {}^3i_q \end{bmatrix} \tag{21}$$

where $\mathbf{K_{OC}}$ consists of the healthy columns of $\mathbf{K_{dq}}$. The solution to this problem is:

$$\begin{bmatrix} {}^2i_d \\ {}^2i_q \\ {}^3i_d \\ {}^3i_q \end{bmatrix} = \mathbf{K_{OC}}'(\theta_e)\left[\mathbf{K_{OC}}(\theta_e)\mathbf{K_{OC}}'(\theta_e)\right]^{-1}\mathbf{w}^* = \mathbf{K}_{\mathbf{OC}}^{+}(\theta_e)\mathbf{w}^* \tag{22}$$

The solution resembles that of normal operation, but the challenges associated with computing this matrix will be addressed in future publications, even though open-circuit faults are well-documented in the literature.

For short-circuit faults, several issues arise. First, the short-circuit current must be located. Second, an estimation of this current must be computed to correct the force reference. However, current estimators, particularly for inter-turn short-circuits, lack the precision required to handle this effectively.

5. Conclusion

This study has delved into the complexities and advancements in the control of MSPM machines, focusing on the computation of current references for effective torque and force control. The integration of bearingless technology with traditional rotating electric machines offers significant advantages, including reduced mechanical losses and enhanced reliability, making them suitable for high-speed applications such as compressors, flywheels, and high-speed generators.

The discussion covered two techniques for addressing the inversion problem in MSPM machine control: the Decoupled Torque and Force Control Technique and the Pseudo-inverse Calculation. Each technique presents unique benefits and challenges. The Decoupled Torque and Force Control Technique simplifies control by separating torque and force but introduces ripples that require additional corrections. Conversely, the Pseudo-inverse Calculation minimizes Joule losses and efficiently determines current references but faces computational complexity, necessitating offline precomputation and storage in lookup tables.

An examination was also conducted on how eccentricity impacts force generation and the strategies available for its compensation. These strategies include mechanical loop correction and explicit correction in the wrench model. Such advancements underscore the growing maturity of MSPM machine control systems, facilitating the integration of new functionalities like power-sharing and fault-tolerant control.

In power-sharing configurations, dynamic allocation of current among sectors enhances load balancing and efficiency. For fault-tolerant control, particularly in handling open-circuit and short-circuit conditions, innovative strategies have been proposed to maintain system stability and performance. However, challenges remain, particularly in the precise estimation and correction of short-circuit currents.

Overall, the advancements in MSPM machine control strategies underscore the potential for these machines in various high-performance applications. Future research should focus on addressing the remaining challenges, particularly in computational efficiency and fault correction, to further enhance the robustness and reliability of MSPM machines.

References

[1]A. Chiba et al. *Magnetic Bearings and Bearingless Drives*. Elsevier, 2005.

[2]Christian Brecher et al. “Design of an aircraft generator with radial force control.” In: *Open Research Europe* 2 (2023). DOI: 10.12688/openreseurope.14684.3.

[3]Alexander H. Pesch et al. “Magnetic Bearing Spindle Tool Tracking Through μ -Synthesis Robust Control”. In: *IEEE/ASME Transactions on Mechatronics* 20.3 (2015), pp. 1448–1457. DOI: 10.1109/TMECH.2014.2344592.

[4]Junichi Asama et al. “A design consideration of a novel bearingless disk motor for artificial hearts”. In: *2009 IEEE Energy Conversion Congress and Exposition*. 2009, pp. 1693–1699. DOI: 10.1109/ECCE.2009.5316302.

[5]K. Inagaki et al. “Performance characteristics of inset-type permanent magnet bearingless motor drives”. In: *2000 IEEE Power Engineering Society Winter Meeting. Conference Proceedings (Cat. No.00CH37077)*. Vol. 1. 2000, 202–207 vol.1. DOI: 10.1109/PESW.2000.849955.

[6]S. Kobayashi, M. Ooshima, and M. Nasir Uddin. “A radial position control method of bearingless motor based on d-q axis current control”. In: *2011 IEEE Industry Applications Society Annual Meeting*. 2011, pp. 1–8. DOI: 10.1109/IAS.2011.6074331.

[7]G. Valente et al. “Radial Force Control of Multisector Permanent-Magnet Machines for Vibration Suppression”. In: *IEEE Transactions on Industrial Electronics* 65.7 (2018), pp. 5395–5405. DOI: 10.1109/TIE.2017.2780039.

[8]G. Valente et al. “Radial force control of multi-sector permanent magnet machines”. In: (2016), pp. 2595–2601. DOI: 10.1109/ICELMACH.2016.7732887.

[9]Huifeng Cui and Xiaofeng Ding. “Suspension Force Model of Bearingless Multi-Sector Surface-Mounted Permanent Magnet Synchronous Motor Based on Maxwell Stress Tensor Method”. In: *2023 26th International Conference on Electrical Machines and Systems (ICEMS)*. 2023, pp. 3163–3168. DOI: 10.1109/ICEMS59686.2023.10344521.

[10]M. Ooshima, S. Kobayashi, and M. Nasir Uddin. “Magnetic levitation tests of a bearingless motor based on d-q axis current control”. In: *2012 IEEE Industry Applications Society Annual Meeting*. Las Vegas, NV, USA: IEEE, Oct. 2012, pp. 1–7. DOI: 10.1109/IAS.2012.6374033.

[11]M. Ooshima, T. Karasawa, and M. Nasir Uddin. “Stabilized control strategy under loaded conditions in a bearingless motor based on d-q axis current control”. en. In: *2013 IEEE Industry Applications Society Annual Meeting* (Oct. 2013), pp. 1–7. DOI: 10.1109/IAS.2013.6682515. (Visited on 01/24/2025).

[12]G. Valente et al. “Radial force control of Multi-Sector Permanent Magnet machines considering radial rotor displacement”. In: *2017 IEEE Workshop on Electrical Machines Design, Control and Diagnosis (WEMDCD)*. 2017, pp. 140–145. DOI: 10.1109/WEMDCD.2017.7947737.

[13]Giorgio Valente et al. “Performance Improvement of Bearingless Multisector PMSM With Optimal Robust Position Control”. In: *IEEE Transactions on Power Electronics* 34.4 (2019), pp. 3575–3585. DOI: 10.1109/TPEL.2018.2853038.

[14]Giacomo Sala et al. “Power-Sharing Control in Bearingless Multi-Sector and Multi-Three-Phase Permanent Magnet Machines”. In: *IEEE Transactions on Industrial Electronics* 68.10 (2021), pp. 9070–9080. DOI: 10.1109/TIE.2020.3026273.

[15]Zhuang Wen et al. “Modular Power Sharing Control for Bearingless Multithree Phase Permanent Magnet Synchronous Machine”. en. In: *IEEE Transactions on Industrial Electronics* 69.7 (July 2022), pp. 6600–6610. DOI: 10.1109/TIE.2021.3097610.

[16]Bo Wang et al. “Advanced Fault Tolerant 3×3-phase PM Drive with Concentric Winding for EV Application”. en. In: *IEEE Transactions on Transportation Electrification* (2022), pp. 1–1. ISSN: 2332-7782, 2372-2088. DOI: 10.1109/TTE.2022.3227621. URL: https://ieeexplore.ieee.org/document/9975309/ (visited on 12/09/2022).

[17]Masahide Ooshima, Ayumu Kobayashi, and Takayoshi Narita. “Stabilized suspension control strategy at failure of a motor section in a d-q axis current control bearingless motor”. In: *2015 IEEE Industry Applications Society Annual Meeting*. Addison, TX, USA: IEEE, Oct. 2015, pp. 1–7. DOI: 10.1109/IAS.2015.7356813.